Atlantic ocean heat transport enabled by Indo-Pacific heat uptake and mixing

Ryan M. Holmes[1,2], Jan D. Zika[2], Raffaele Ferrari[3], Andrew F. Thompson[4], Emily R. Newsom[5], and Matthew H. England[1]

[1]Climate Change Research Centre and the ARC Centre of Excellence for Climate Extremes, University of New South Wales, Sydney, NSW, Australia
[2]School of Mathematics and Statistics, University of New South Wales, Sydney, NSW, Australia
[3]Department of Earth, Atmosphere and Planetary Sciences, Massachusetts Institute of Technology, Cambridge, Massachusetts, U.S.A.
[4]Environmental Science and Engineering, California Institute of Technology, Pasadena, California, U.S.A.
[5]Department of Physics, University of Oxford, Oxford, United Kingdom

Key Points:

- Heat budget analysis reveals links between meridional and diathermal ocean heat transports
- Atlantic northward heat transport sourced from eastern tropical Pacific heat uptake
- Turbulent mixing transfers heat from warm shallow Indo-Pacific circulation to cold deep-reaching Atlantic circulation

Corresponding author: Ryan Holmes, `ryan.holmes@unsw.edu.au`

Abstract

The ocean transports vast amounts of heat around the planet, helping to regulate regional climate. One important component of this heat transport is the movement of warm water from equatorial regions toward the poles, with colder water flowing in return. Here, we introduce a framework relating meridional heat transport to the diabatic processes of surface forcing and turbulent mixing that move heat across temperature classes. Applied to a $1/4°$ global ocean model the framework highlights the role of the tropical Indo-Pacific in the global ocean heat transport. A large fraction of the northward heat transport in the Atlantic is ultimately sourced from heat uptake in the eastern tropical Pacific. Turbulent mixing moves heat from the warm, shallow Indo-Pacific circulation to the cold deeper-reaching Atlantic circulation. Our results underscore a renewed focus on the tropical oceans and their role in global circulation pathways.

1 Introduction

The ocean plays a critical role in the climate system by moving heat between climate zones and sequestering it in the subsurface (Gregory, 2000; Trenberth & Caron, 2001; Trenberth, Zhang, Fasullo, & Cheng, 2019). How this heat transport responds to external forcing due to interannual and decadal natural variability and forced climate change remains a first-order question in climate science.

Studies of ocean heat transport have traditionally focused on the ocean's general circulation (i.e. the circulation of seawater), and how it carries heat with it. The drivers of this circulation still remain under discussion, with debate centering around the proportion of water-mass transformation between light and dense waters occurring in the high-latitude North Atlantic and the Southern Ocean and through diapycnal upwelling at lower latitudes (Cessi, 2019; Ferrari, Nadeau, Marshall, Allison, & Johnson, 2017; Ferrari & Wunsch, 2009; Gnanadesikan, 1999; Lee et al., 2018; Marshall & Speer, 2012; Newsom & Thompson, 2018; L. Talley, 2013; Thompson, Stewart, & Bischoff, 2016; Toggweiler, Druffel, Key, & Galbraith, 2019). Some studies emphasize the importance of an inter-basin circulation involving significant exchange of water of differing densities between the Atlantic and Indo-Pacific basins (Ferrari et al., 2017; Thompson et al., 2016) through the Southern Hemisphere super-gyre (Gordon, 1986; Gordon, Weiss, Smethie Jr., & Warner, 1992; Rintoul, 1991; Speich, Blanke, & Cai, 2007). In particular, Newsom and Thompson (2018) highlighted the importance of asymmetries in the net buoyancy forcing between the Atlantic and Indo-Pacific, emphasizing the often overlooked role of water-mass transformation in the tropical Indo-Pacific for the global residual circulation. However, as emphasized by Forget and Ferreira (2019), connecting ocean heat transport only with the circulation of seawater can be problematic as much of the heat content within a given water parcel remains inaccessible for ocean-atmosphere exchange and simply moves around closed circulation loops, such as the horizontal gyres, unchanged.

The ocean is warmed by air-sea heat fluxes at low-latitudes and warm sea surface temperatures, and cooled in the mid- and high-latitudes at colder temperatures (e.g. W. G. Large & Yeager, 2009; Speer & Tziperman, 1992; Valdivieso et al., 2017). Therefore, in order to maintain a steady state, heat must be moved not only from low to high latitudes (the ocean's *meridional* heat transport), but also from warm to cold temperatures (the ocean's *diathermal* heat transport). This net down-gradient warm-to-cold heat transfer can only be achieved by diffusive mixing processes (e.g. Hieronymus, Nilsson, & Nycander, 2014; Niiler & Stevenson, 1982), which act to destroy the temperature differentials created by air-sea heat fluxes. Holmes, Zika, and England (2019a, hereafter HZE19) showed in a global ocean sea-ice model that this down-gradient diathermal heat transport peaks near 22°C with a magnitude similar to the peak meridional heat transport. This realization highlights the dependence of the ocean's meridional heat transport on diabatic processes[1], both surface forcing and turbulent mixing, that influence the temperature of waters that are exchanged across latitude lines by the circulation. However, no comprehensive description of oceanic heat transport pathways that includes diathermal transports yet exists.

A number of studies have attempted to attribute the ocean's meridional heat transport to different aspects of the ocean circulation by introducing various forms of *heat functions* (e.g. Boccaletti, Ferrari, Adcroft, Ferreira, & Marshall, 2005; Czaja & Marshall, 2006; Ferrari & Ferreira, 2011; Greatbatch & Zhai, 2007; Saenko, Yang, & Gregory, 2018; Vallis & Farneti, 2009; Yang, Li, Wang, Sun, & Sun, 2015; Zika, Laliberté, Mudryk, Sijp, & Nurser, 2015; Zika, Sijp, & England, 2013). Such heat functions quantitatively isolate net ocean heat transports from the passive circulation of heat around closed circulation cells (also see L. D. Talley, 2003, for an alternative approach based on water-masses). Ferrari and Ferreira (2011) used a heat function to demonstrate that the ocean's meridional heat transport is controlled largely by winds and mixing within the thermocline, and is less sensitive to high-latitude convection or abyssal mixing, which form the traditional focus of studies of the ocean's overturning. While the deep-reaching Atlantic Meridional Overturning Circulation (AMOC) does carry large amounts of heat northward, it remains unclear how and where this heat is supplied, and how the deep-reaching circulation is connected to the shallow wind-driven cells that otherwise dominate the heat transport.

The heat function of Ferrari and Ferreira (2011) provides an intuitive framework in which to evaluate the contribution of different aspects of ocean circulation to the ocean's meridional heat transport. By constructing a complete budget for the heat function in the latitude-temperature plane (Section 2) we will show that a similar framework can be used to evaluate the role of different diabatic processes. We apply this budget framework to a comprehensive 1/4° global ocean sea-ice model to evaluate the contribution of diabatic processes occurring in different ocean basins to the ocean's meridional heat transport (Sections 3 and 4). We find that, while much of the ocean's northward heat transport occurs in the Atlantic ocean, Indo-Pacific diabatic processes play a critical role by connecting the shallow and deep circulations and providing heat to the AMOC to be carried northward (Section 5). Our results are summarized in Section 6.

2 A framework for studying ocean heat transport

In this section we describe an extension of the global diathermal heat transport framework discussed by HZE19 that can be used to study the flow of heat in the temperature-latitude plane.

2.1 Internal heat content

We consider the heat budget of the volume of fluid colder than a given temperature Θ and bounded to the north by a latitude ϕ (Fig. 1). The volume[2] of this region is,

$$\mathcal{V}(\phi, \Theta, t) = \int\int\int_{\Theta'(x',\phi',z',t)<\Theta} H(\phi - \phi')dV', \tag{1}$$

[1] Here we define a diabatic process as any process that changes the temperature of a fluid parcel, including the along-isopycnal diffusive transport of heat resulting from eddy stirring.

[2] Our study will be performed in the context of incompressible Boussinesq model simulations. If the fluid were instead compressible then it would be more appropriate to consider the mass rather than volume (Hochet & Tailleux, 2019; Holmes, Zika, & England, 2019b).

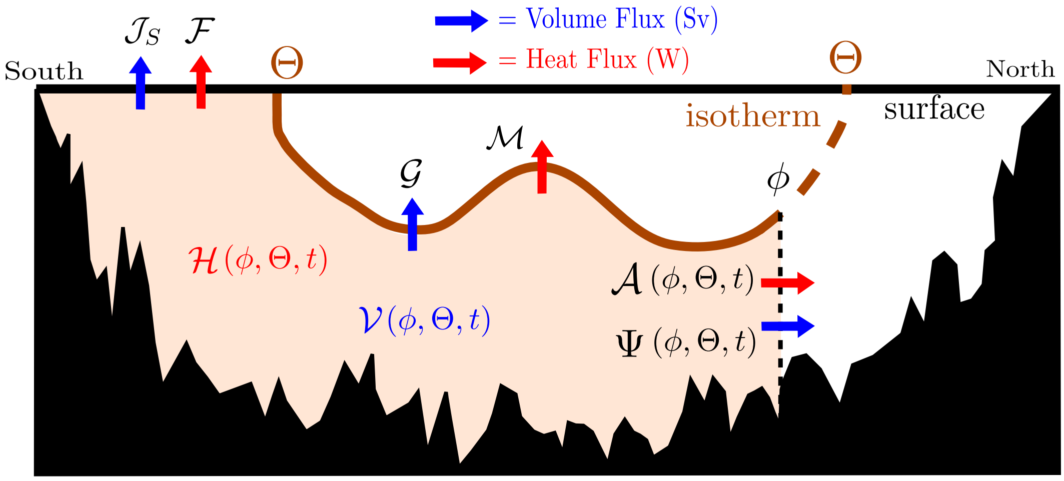

Figure 1. A schematic illustrating the heat and volume budgets of all water colder than some temperature Θ (marked by the brown isotherm) and south of some latitude ϕ (black dashed line). The volume $\mathcal{V}$ and heat content $\mathcal{H}$ of this region are functions of Θ, ϕ and time t. All fluxes are also functions of Θ, ϕ and t and are defined as positive if they are out of the volume $\mathcal{V}$. $\mathcal{F}$ denotes the surface heat fluxes (including the heat flux associated with the surface volume flux $\mathcal{J}_S$) and $\mathcal{M}$ denotes the heat fluxes across the Θ isotherm due to explicitly-parameterized vertical mixing and numerical mixing. $\mathcal{G}$ denotes the volume flux across the Θ isotherm associated with water-mass transformation. There are also volume $\Psi(\phi,\Theta,t)$ and heat $\mathcal{A}(\phi,\Theta,t)$ fluxes across the northern bounding latitude ϕ.

where H is the Heaviside step function and the integral is performed following the temporally- and spatially-varying temperature field Θ'. The heat content of this volume $\mathcal{H}$ can be represented in terms of an integral in temperature coordinates,

$$\mathcal{H}(\phi,\Theta,t) = \int_{-\infty}^{\Theta} \rho_0 C_p \Theta' \frac{\partial \mathcal{V}}{\partial \Theta'} d\Theta', \tag{2}$$

where ρ_0 is a constant reference density, C_p is a constant 'specific heat capacity'[3], and $\frac{\partial \mathcal{V}}{\partial \Theta'} d\Theta'$ represents the volume within a given temperature interval $d\Theta'$ south of ϕ. Following HZE19, $\mathcal{H}$ can be integrated by parts and split into an external component,

$$\mathcal{H}_E(\phi,\Theta,t) = \rho_0 C_p \Theta \mathcal{V}, \tag{3}$$

and an internal component,

$$\mathcal{H}_I(\phi,\Theta,t) = -\rho_0 C_p \int_{-\infty}^{\Theta} \mathcal{V} d\Theta' = \rho_0 C_p \left(\overline{\Theta} - \Theta\right) \mathcal{V}, \tag{4}$$

where $\mathcal{H} = \mathcal{H}_I + \mathcal{H}_E$ and the last identity follows from $\mathcal{H} = \rho_0 C_p \overline{\Theta} \mathcal{V}$ where $\overline{\Theta} = \frac{1}{\mathcal{V}} \int_{-\infty}^{\Theta} \Theta' (\partial \mathcal{V}/\partial \Theta') d\Theta'$ is the volume averaged temperature. The internal component $\mathcal{H}_I$ is the heat content associated with the difference between the volume average temperature and the bounding temperature Θ (meaning that here $\mathcal{H}_I$ is always negative). Because of its dependence on a temperature difference, $\mathcal{H}_I$ is independent of the zero reference chosen for the temperature scale. In addition, the transport of $\mathcal{H}_I$ across the latitude ϕ, defined as $\mathcal{A}_I$ below, can be identified as the heat function of Ferrari and Ferreira (2011).

[3] Note that the simulations we consider use potential temperature with a constant for C_p and thus make the assumption that potential temperature is conserved within the ocean, which is not strictly the case (McDougall, 2003). However, with a variable $C_p\Theta$ all results would follow similarly.

2.2 Transport of internal heat content

The volume transport below the Θ isotherm defines a temperature stream function,

$$\Psi(\phi, \Theta, t) = \int \int_{\Theta'(x,\phi,z,t)<\Theta} v(x, \phi, z, t) dx dz, \tag{5}$$

where v is the meridional velocity (including any parameterized eddy-driven circulation) and the integral is performed following the time-varying temperature field Θ' at the latitude ϕ. The associated northward heat transport in Watts relative to 0°C is,

$$\mathcal{A}(\phi, \Theta, t) = \int_{-\infty}^{\Theta} \rho_0 C_p \Theta' \frac{\partial \Psi}{\partial \Theta'} d\Theta' + \mathcal{A}_D(\phi, \Theta, t), \tag{6}$$

where $\frac{\partial \Psi}{\partial \Theta'} d\Theta'$ represents the volume transport within a temperature interval $d\Theta'$ and $\mathcal{A}_D$ indicates any meridional heat transport that is not associated with the volume transport Ψ (for example, the meridional component of parameterized diffusion).

The heat transport [Eq. (6)] can be integrated by parts, as for the heat content [Eq. (2)], and split into an external component,

$$\mathcal{A}_E(\phi, \Theta, t) = \rho_0 C_p \Theta \Psi, \tag{7}$$

and an internal component,

$$\mathcal{A}_I(\phi, \Theta, t) = -\rho_0 C_p \int_{-\infty}^{\Theta} \Psi d\Theta' + \mathcal{A}_D, \tag{8}$$

where $\mathcal{A} = \mathcal{A}_E + \mathcal{A}_I$. $\mathcal{A}_E$ would be the total heat transport if all of the fluid below Θ was isothermal. Thus the internal component $\mathcal{A}_I$ captures the heat transport associated with variations in temperature within the layer. Once again, the internal heat content transport $\mathcal{A}_I$ is independent of the reference temperature used to define heat content, and contributes to a simpler budget (see Section 2.3). Note that the diffusive meridional heat transport $\mathcal{A}_D$ is part of $\mathcal{A}_I$ as it is not associated with a volume transport and depends only on temperature differences.

The internal heat content transport $\mathcal{A}_I$ in Eq. (8) is equivalent to the heat function of Ferrari and Ferreira (2011) (note that we use the opposite sign for Ψ). Differencing the heat function across a given circulation cell yields the meridional heat transport attributable to that cell. Evaluating the heat function at the maximum SST, $\Theta^{max}(\phi, t)$ (across all longitudes and seasons), captures the full depth circulation and thus yields the total meridional heat transport,

$$MHT(\phi, t) = \mathcal{A}_I(\phi, \Theta^{max}, t). \tag{9}$$

The total external heat transport, $\mathcal{A}_E(\phi, \Theta^{max}, t)$ is not included as it depends on the arbitrary reference temperature. Heat transport in the presence of a net volume transport is discussed in more detail in supplementary text S3.

2.3 Diabatic contributions to $\mathcal{A}_I$

The heat function $\mathcal{A}_I$ can also be related to the diabatic processes that alter the temperature of seawater parcels, leading to diathermal heat transports that contribute to the heat budget of the volume $\mathcal{V}$. The full heat content budget for this volume is (Fig. 1),

$$\frac{\partial \mathcal{H}}{\partial t}(\phi, \Theta, t) = -\mathcal{F} - \mathcal{M} - \mathcal{A} - \rho_0 C_p \Theta \mathcal{G}, \tag{10}$$

where $\mathcal{F}$ denotes the heat flux out of the volume $\mathcal{V}$ associated with surface forcing, $\mathcal{A}$ is the heat transport across the latitude ϕ [Eq. (6)], $\mathcal{M}$ denotes the heat flux across the

Θ isotherm associated with mixing processes and the last term is the heat flux associated with the volume flux across the Θ isotherm, $\mathcal{G}$. Following HZE19, Eq. (10) can be combined with the volume budget (Fig. 1),

$$\frac{\partial \mathcal{V}}{\partial t}(\phi, \Theta, t) = -\mathcal{J}_S - \mathcal{G} - \Psi, \tag{11}$$

where $\mathcal{J}_S$ is the surface volume flux out of the volume $\mathcal{V}$, to yield a budget for the internal heat content [use Eq. (11) to substitute for $\mathcal{G}$ in Eq. (10)],

$$\frac{\partial \mathcal{H}_I}{\partial t}(\phi, \Theta, t) = -\mathcal{F}_I - \mathcal{M} - \mathcal{A}_I. \tag{12}$$

In Eq. (12), $\mathcal{F}_I = \mathcal{F} - \rho_0 C_p \Theta \mathcal{J}_S$ denotes the surface forcing corrected for the reference temperature dependent heat flux associated with surface volume fluxes (see HZE19 for more discussion). The internal heat content budget is not influenced by the volume flux across the Θ isotherm $\mathcal{G}$. This will be particularly important when analyzing the heat transport within the Atlantic or Indo-Pacific basins individually where $\mathcal{G}$ may be large, and it is not clear how to robustly assign a value of heat transport to it given its dependence on the reference temperature [Eq. (10)].

The budget Eq. (12) quantifies the relationship between the ocean's meridional heat transport, heat content tendency and the diabatic processes of surface forcing and mixing integrated over the volume $\mathcal{V}$. It can often be easier to interpret this budget by examining its local form that applies to a given infinitesimal region in the latitude-temperature plane [i.e. taking the Θ and ϕ derivative of Eq. (12)],

$$\frac{\partial}{\partial t}\left(\frac{\partial^2 \mathcal{H}_I}{\partial \Theta \partial \phi}\right) = -\frac{\partial}{\partial \Theta}\underbrace{\left(\frac{\partial \mathcal{F}_I}{\partial \phi} + \frac{\partial \mathcal{M}}{\partial \phi}\right)}_{\mathcal{J}_\Theta} - \frac{\partial}{\partial \phi}\underbrace{\left(\frac{\partial \mathcal{A}_I}{\partial \Theta}\right)}_{\mathcal{J}_\phi}, \tag{13}$$

where $\mathcal{J}_\Theta$ and $\mathcal{J}_\phi$ denote the local diathermal and meridional heat fluxes respectively. Note that some processes, such as the along-isopycnal diffusion of temperature associated with eddy stirring, may have both a diathermal and a meridional [through $\mathcal{A}_D$ in Eq. (8)] component.

2.4 Global ocean sea-ice model

We explore the heat transport and its dependence on diabatic processes using the *MOM025 Control* 1/4° global ocean sea-ice model used in HZE19. The model configuration is based on the ocean and sea-ice components of the GFDL CM2.5 climate model (Delworth et al., 2012) and has 50 vertical levels. Repeating seasonally-varying atmospheric forcing is taken from version 2 of the Coordinated Ocean-ice Reference Experiment Normal Year Forcing (CORE-NYF, W. Large & Yeager, 2004). MOM025 Control does not include a parameterization for lateral or along-isopycnal temperature diffusion. Small-scale lateral temperature gradients are diffused by the numerical advection scheme, which is included in the mixing term $\mathcal{M}$ (see supplementary text S2). The heat function and budget terms in Eqs. (12)-(13) are diagnosed from the model heat budget terms binned online, at every time step, into 0.5°C temperature bins. The details of these calculations, along with more information on the model configuration, are described in supplementary text S1 and in HZE19.

3 The temperature structure of heat transport

The global stream function for volume transport in the temperature-latitude plane (Fig. 2a) consists of an Antarctic Bottom Water (AABW) cell south of 50°S, a North Atlantic Deep Water (NADW) cell between temperatures of 3°C and 12°C and northern and southern shallow subtropical cells at warmer temperatures. While all four cells carry a similar magnitude mass transport (reaching 20−30Sv), the two deep cells cover a narrower temperature range and thus contribute less to the heat transport. This heat transport is quantified by the heat function $\mathcal{A}_I$ (Fig. 2d). $\mathcal{A}_I$ contours describe the entrance of heat into the ocean at low latitudes, its movement poleward while descending toward colder temperatures, and the subsequent loss of heat back to the atmosphere at mid- and high-latitudes. In the meridional direction, this contour-following heat transport should be interpreted as the net effect of water moving in different directions at different temperatures. The net northward transport of internal heat content reaches 1.5PW near 20°N, with a smaller southward maximum of 0.6PW in the Southern Hemisphere (Fig. 2d at warmest temperature, black line in Fig. 3).

The heat function suggests that a large fraction of the meridional heat transport is achieved at warmer temperatures, where heat is supplied to the circulation (Fig. 2d). The subtropical cells, which include components due to both vertical overturning and horizontal gyre circulation[4], play a major role as they span the large temperature range of all waters warmer than $\sim 12°$C (Ferrari & Ferreira, 2011; Klinger & Marotzke, 2000). While much of this heat transport occurs at temperatures that may be exposed to the atmosphere at some longitude and season (i.e. above the lower dotted black line in Fig. 2 that indicates the minimum SST at each latitude), there is also a significant fraction that is associated with interior flow. In particular, at low-latitudes heat function contours have a downward, across-isotherm slope indicating the presence of interior diabatic processes. In contrast, the heat function contours at still colder temperatures associated with the NADW cell (below $\sim$ 10°C in Fig. 2d) are more isothermal, indicating that diabatic processes are weaker.

Decomposing the global circulation into contributions from the Atlantic (Fig. 2b,e) and Indo-Pacific (Fig. 2c,f) reveals a story that is obscured in the global view. In a temperature coordinate the Indo-Pacific circulation consists largely of the two subtropical cells, with the Southern Hemisphere cell being stronger (due to stronger peak wind stresses in the Southern Hemisphere westerlies, Cessi, 2019; Speich et al., 2007) and spanning a larger temperature range. In contrast, the Atlantic is characterized by a clockwise circulation encompassing both the subtropical surface and NADW deep cells. These features have important implications for the heat transport in the two basins. The Atlantic transports heat northward at all latitudes (red line in Fig. 3, also see Ganachaud & Wunsch, 2003), with both deep and surface circulations contributing (Fig. 2e Ferrari & Ferreira, 2011; L. D. Talley, 2003). In contrast the heat transport in the Pacific is more surface intensified while still overlapping in temperature with the Atlantic circulation in the Southern Hemisphere (Fig. 2f, blue line in Fig. 3). The southward heat transport out of the subtropical Indo-Pacific across 34°S exceeds the global southward heat transport there (compare black and blue lines in Fig. 3), meaning that a significant fraction of this heat ($\sim$ 0.5PW) must ultimately be a source for the northward heat transport in the Atlantic. The spatial structure of the surface heat flux implies that there must be a large transfer of heat from the Indo-Pacific to the Atlantic basin (also see Gordon, 1986), but, as discussed in the next section, this in turn requires that turbulent mixing diffuses heat into the temperature classes that experience net cooling in the surface North Atlantic. Note that the net heat transports in the individual basins (Fig. 3), as well as the temperature structure of these transports (Fig. 2), compare well with the buoyancy transports discussed by Newsom and Thompson (2018, their Figs. 2 and 4) outside the high-latitude Southern Ocean, showing that heat transport generally dominates the buoyancy transport in the upper ocean in these regions.

[4] We do not attempt to decompose the heat transport into horizontal and vertical components in this study. Such a decomposition has been attempted elsewhere (e.g. Boccaletti et al., 2005).

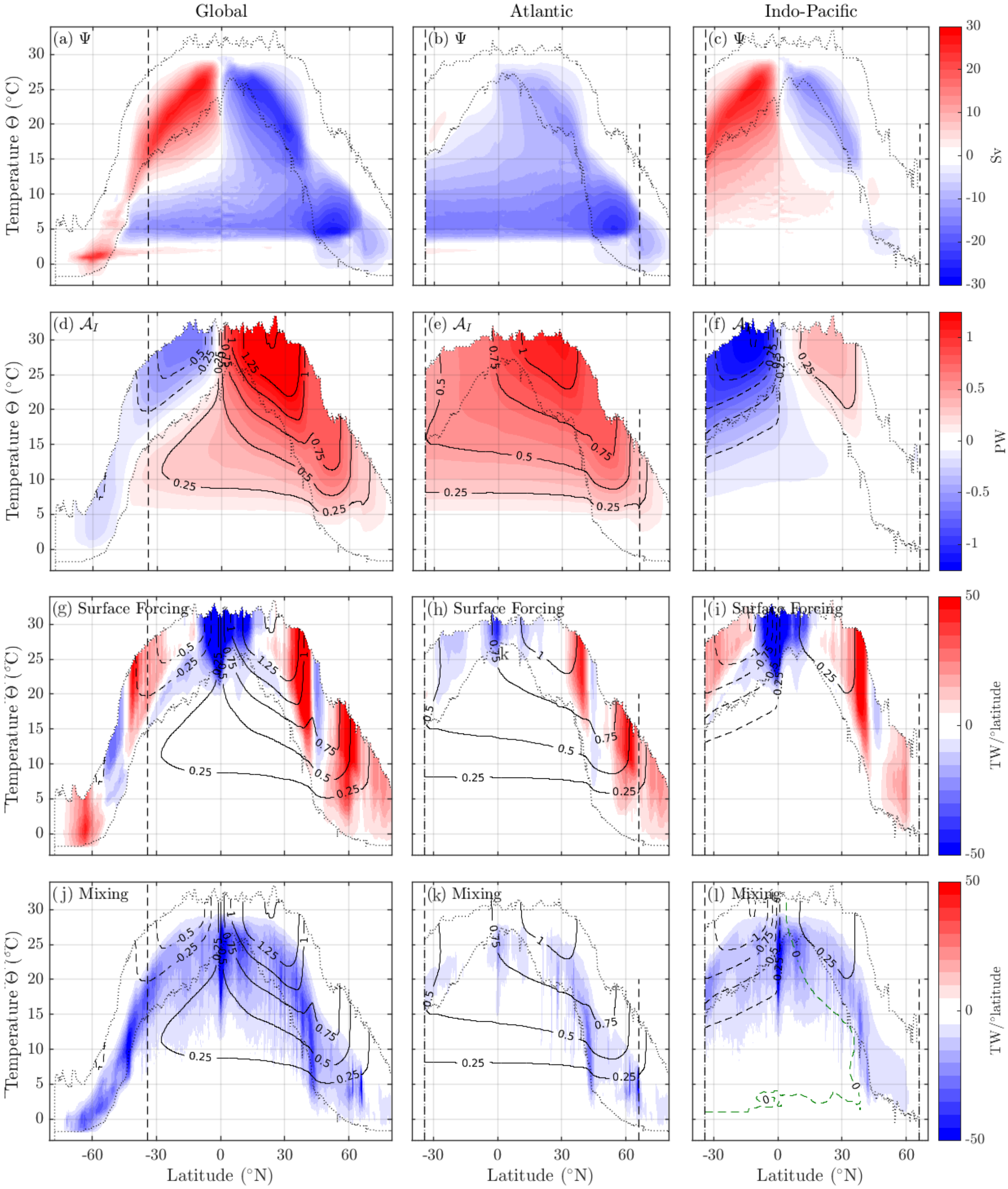

Figure 2. MOM025 Control (a-c) residual stream function Ψ in temperature coordinates [Eq. (5), Sv], (d-f) heat function $\mathcal{A}_I$ [Eq. (8), PW] and diathermal heat transports (TW/° latitude) due to (g-i) surface forcing [$\partial\mathcal{F}_I/\partial\phi$ in Eq. (13)] and (j-l) mixing [$\partial\mathcal{M}/\partial\phi$ in Eq. (13)] for (left column) all basins, (middle column) the Indo-Pacific and (right column) the Atlantic. The thin dotted lines mark the minimum and maximum SST at each latitude at all zonal locations and seasons within the respective basin. The boundaries between the various basins are indicated by vertical dashed lines (including the Bering Strait at 66°N). The Arctic ocean is included in the Atlantic. In panels g-l blue colors indicate fluxes toward colder temperature and the heat function $\mathcal{A}_I$ is shown in thin 0.25PW contours for each basin, with the solid (dashed) contours indicating positive (negative) values.

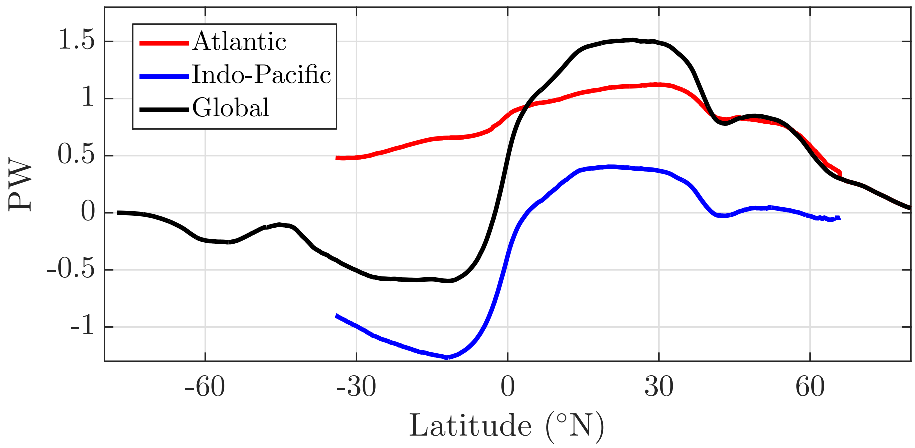

Figure 3. MOM025 Control global meridional heat transport (Eq. (9), PW, black line) and its Atlantic (red) and Indo-Pacific (blue) components.

4 Diabatic contributions to heat transport

The net transport of heat from low- to high-latitudes captured by the heat function $\mathcal{A}_I$ could not occur without heat transport across temperature classes quantified by the diathermal heat flux $\mathcal{J}_\Theta$. $\mathcal{J}_\Theta$, the vertical vector component of the heat function contours in the temperature-latitude plane [Eq. (13)], contains contributions from surface forcing (Fig. 2g-i) and mixing (Fig. 2j-l). Surface heating in the equatorial regions between $\pm 15°$ latitude acts as the main source of heat to the ocean circulation (Fig. 2g). This heat uptake is dominated by the eastern equatorial Pacific cold tongue (1.09PW of heat enters the region 10°S-10°N, $165° - 70°$W, not shown, see Fig. 1a of HZE19), with a much smaller fraction entering the low-latitude Atlantic (0.36PW between 10°S-10°N across the Atlantic, compare Figs. 2g-i, also see Newsom & Thompson, 2018). However, the Atlantic contributes much more substantially to surface heat loss. Much of this heat loss occurs poleward of 50°N (0.7PW, compared to 0.11PW north of 50°N in the Indo-Pacific), with heat loss also dominating over the Gulf Stream between 30°N and 45°N. Thus to maintain a steady state (the tendency in heat content is weak, Fig. S1), the ocean circulation must arrange itself to connect the regions of heat gain and heat loss by exporting heat from the Indo-Pacific to the Atlantic. Note that the two-dimensional structure of the surface heat flux in the Southern Ocean indicates that heat loss in one zonal sector is not balanced by heat gain in another sector (not shown, see Fig. 1a of HZE19), further supporting the need for inter-basin heat exchange.

The patterns of surface heat uptake and surface heat loss imply not only a transport of heat from low-latitudes to high-latitudes and from the Indo-Pacific to the Atlantic, but also from warm to cold temperatures (HZE19). The hot spot of heat loss in the high-latitude North Atlantic occurs at temperatures well below 18°C, the maximum surface temperature there (Fig. 2h), while low-latitude heating penetrates only to about 20°C (Fig. 2g). This highlights the essential role of mixing (Fig. 2j-l, Speer & Tziperman, 1992). It is only through mixing that the regions of surface heat gain and loss can be connected, allowing heat to reach the cool isotherms that outcrop in the North Atlantic. Mixing accounts for much of the downward slope in the heat function contours within the cool branch of the subtropical cells. Without this mixing, the circulation cells would span a reduced temperature range and thus without a compensating increase in volume transport would transport less heat (Czaja & Marshall, 2006).

Much of the mixing, particularly at warmer temperatures, occurs in the Indo-Pacific basin (compare Figs. 2j,l). This mixing contains contributions from a number of explicitly-parameterized vertical mixing processes and numerical mixing, as discussed in more detail in supplementary text S2 and HZE19. Mixing is less important in the Atlantic, where heat function contours follow more isothermal pathways (Fig. 2k). The Southern Ocean appears to play a secondary role when considering heat transport alone (Fig. 2j), as opposed to density-based water-mass transformation. The diathermal heat flux associated with mixing is particularly strong at ±40° latitude. This is largely associated with numerical mixing (supplementary Fig. S2d), and likely reflects the important role of mesoscale eddy stirring of along-isopycnal temperature gradients at these latitudes. If explicitly parameterized, this along-isopycnal eddy-stirring would also contribute directly to the meridional heat flux there, in addition to the resolved meridional heat transport in $\mathcal{A}_I$.

5 North Atlantic heat transport across 50°N

The heat transport pathways can be more precisely quantified by examining the total heat transport above and below carefully chosen isotherms. Here we choose the 15°C and 20°C isotherms (Fig. 4), although a similar analysis could easily be applied to other isotherms. 20°C is chosen because it represents the coldest isotherm to which surface heating penetrates in the tropics (Fig. 2g). 15°C is chosen because it captures the majority of the heat transport across 50°N into the North Atlantic, and acts as an upper bound for the NADW overturning cell (Fig. 2h). Approximately 40% (0.35PW) of the 0.78PW of heat transport across 50°N below 15°C in the Atlantic is supplied by surface heat input in the tropical Atlantic followed by mixing across the 20°C and 15°C isotherms. The other 60% (0.49PW) is supplied meridionally across 34°S at temperatures below 15°C. All of this 0.49PW is ultimately sourced from surface heat input at temperatures above 20°C into the tropical Indo-Pacific (totaling 1.22PW, Fig. 4) via a pathway that relies on strong mixing across the 20°C and 15°C isotherms in the Indo-Pacific (1.07 and 0.63PW respectively). Mixing across the 15°C isotherm within the "warm route" latitudes between 45°S and 34°S also contributes (0.27PW).

The passage of heat from the warm tropical Indo-Pacific to the cold North Atlantic is the most obvious pathway in Fig. 4, but other features are also evident. Heat transport into the North Pacific and its subsequent loss to the atmosphere is relatively small (0.19PW below 15°C). Model drift is evident in the build-up of heat below 15°C in the Indo-Pacific (0.1PW). Apart from a modest amount of net heat loss across all three temperature classes (and individually in both the Indo-Pacific and Atlantic sectors of the Southern Ocean, not shown), the high-latitude Southern Ocean appears to play a relatively passive role in the global heat transport (water-mass transformation here is dominated more by freshwater fluxes, e.g. Abernathey et al., 2016). Heat is transported northward throughout the Atlantic with weak net heat exchange with the Southern Ocean above 15°C. There is also a small amount of heat transport through Bering Strait, associated with the 1.03Sv of volume transport from the Pacific into the Arctic. It is difficult to assign a precise value to this heat transport. In supplementary text S3 we argue that its magnitude cannot exceed 0.08PW.

6 Discussion

In this study we have quantified the contribution of different diabatic processes to heat transport in the temperature-latitude plane using a general framework based on the heat function of Ferrari and Ferreira (2011) and the internal heat content budget of HZE19. Applied to a 1/4° global ocean sea-ice model, the framework reveals the dominant global heat transport pathways as summarized in Fig. 4. The ability to construct such a diagram relies on the use of internal heat content, which is independent of any arbitrary reference temperature.

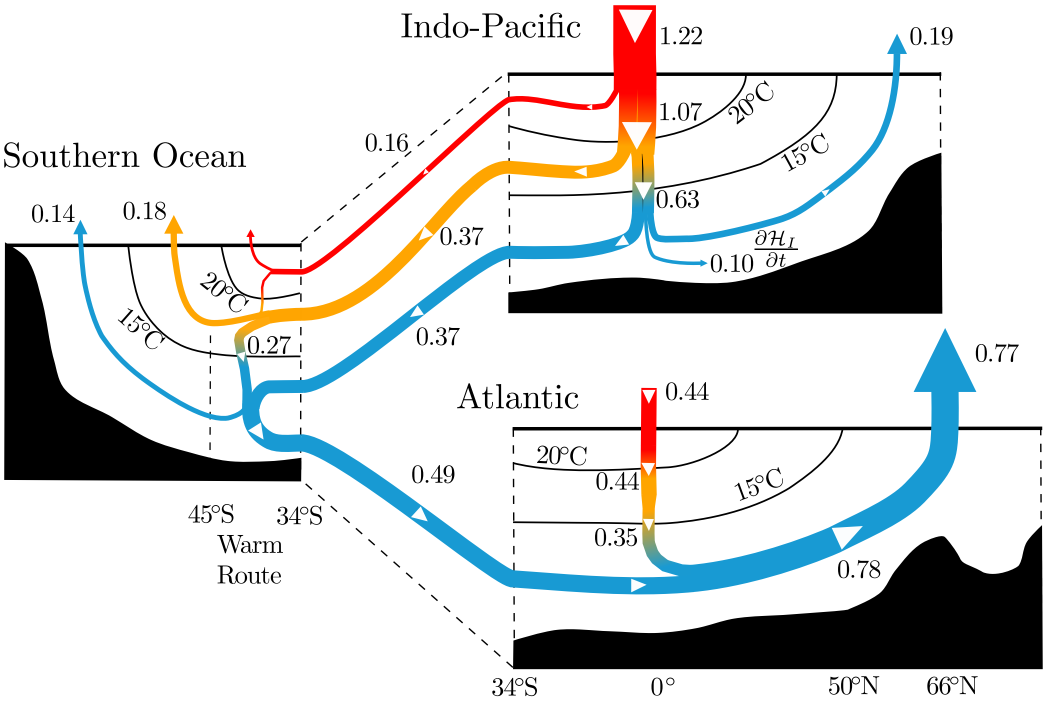

Figure 4. Summary of the internal heat content transports (in PW, with proportional line thickness) above, below and across the 15°C and 20°C isotherm from MOM025 Control. Note that the maximum SST Θ^{max} replaces this upper isotherm bound (either 15°C or 20°C) in the case where it is colder, as described in supplementary text S3. Arrows across the surface represent surface heat fluxes, arrows across the isotherms represent diffusive mixing and horizontal arrows represent meridional internal heat content transports. Note that the isotherm outcrop positions (and the location of many of the heat fluxes) within each basin are somewhat arbitrary as water warmer and colder than 15°C or 20°C contacts the atmosphere over a range of latitudes. Heat transport pathways less than 0.1PW are not shown (these account for the apparent mismatch between pathways).

The dominant heat transport pathway involves the movement of heat from the warm surface waters of the tropical Indo-Pacific (where the majority of warming via surface heat fluxes occurs, Fig. 2g-i, Fig. 1a of HZE19) to the cold North Atlantic where heat is lost back to the atmosphere (Fig. 4). This pathway depends critically on turbulent mixing which transfers heat out of the warm shallow tropical Indo-Pacific waters and supplies the upper branch of the AMOC with heat. 60% of the 0.78PW of meridional heat transport across 50°N in the Atlantic below 15°C is supplied across 34°S at temperatures below 15°C from the Indo-Pacific. As most heat enters the ocean at warmer temperatures, this implies that mixing in the Indo-Pacific (as well as some mixing in the warm route latitudes between 45°S and 34°S) plays a key role in converting NADW back to lighter intermediate and surface waters (e.g. Fig. 2c) permitting the upper branch of the AMOC to transport heat northward.

The large exchange of heat between the Indo-Pacific and Atlantic is consistent with the results of Newsom and Thompson (2018) on buoyancy transport, but differs somewhat from the conclusions of Forget and Ferreira (2019). The results of Forget and Ferreira (2019) suggest net heat fluxes into the Arctic-Atlantic basin of 0.29PW (their Fig. 1), compared to 0.4PW in our study. This difference is linked to the surface heat flux pattern, and highlights the need to improve observational constraints on surface heat fluxes and to compare across a range of models. Analysis in this article is restricted to a single model with a specific set of parameterizations for diabatic processes. A similar MOM configuration with a refined resolution of 1/10° shows a similar fractional contribution of Indo-Pacific heat uptake and mixing to Atlantic meridional heat transport, but does not match observed meridional heat transport estimates as well as MOM025 Control (see supplementary text S4). The framework we have introduced here provides a useful diagnostic tool that could be applied within future model inter-comparisons to assess the sensitivity of ocean heat transport to different parameterizations.

This study highlights the key role of the tropical oceans, and in particular the tropical Indo-Pacific, for global ocean circulation and heat transport. There are a growing number of studies with this emphasis (e.g. Forget & Ferreira, 2019; Newsom & Thompson, 2018; Toggweiler et al., 2019). Here, we stress in particular the role of turbulent mixing in linking the heat transport associated with the shallow wind-driven Indo-Pacific circulation with the deeper-reaching Atlantic overturning circulation. The implications of this connection for the interannual and decadal variability of ocean heat transport remains an important area for future research, especially given the strong natural climate variability present in the tropical Indo-Pacific.

Acknowledgments

We thank A. Heerdegen, S. Griffies and P. Spence for assistance with the modeling and diagnostics. This research was undertaken with the assistance of resources and services from the National Computational Infrastructure (NCI), which is supported by the Australian Government. This project was also supported by the Earth Science and Climate Change Hub of the Australian Government's National Environmental Science Program (NESP) and the Centre for Southern Hemisphere Oceans Research (CSHOR), a joint research centre between QNLM, CSIRO, UNSW and UTAS. The model output and configuration files will be made available through the NCI data portal `http://geonetwork.nci.org.au`.

References

Abernathey, R. P., Cerovecki, I., Holland, P. R., Newsom, E., Mazloff, M., & Talley, L. D. (2016). Water-mass transformation by sea ice in the upper branch of the Southern Ocean overturning. *Nature Geosci*, *9*(8), 596–601.

Boccaletti, G., Ferrari, R., Adcroft, A., Ferreira, D., & Marshall, J. (2005). The vertical structure of ocean heat transport. *Geophys. Res. Lett.*, *32*(10), 1-4. doi: 10.1029/2005GL022474

Cessi, P. (2019). The global overturning circulation. *Annual Review of Marine Science*, *11*(1), 249-270. doi: 10.1146/annurev-marine-010318-095241

Colella, P., & Woodward, P. R. (1984). The piecewise parabolic method (ppm) for gas-dynamical simulations. *J. Comput. Phys.*, *54*(1), 174 - 201. doi: 10.1016/0021-9991(84)90143-8

Czaja, A., & Marshall, J. (2006). The partitioning of poleward heat transport between the atmosphere and ocean. *J. Atmos. Sci.*, *63*(5), 1498–1511. doi: 10.1175/JAS3695.1

Delworth, T. L., Rosati, A., Anderson, W., Adcroft, A. J., Balaji, V., Benson, R., ... Zhang, R. (2012). Simulated climate and climate change in the GFDL CM2.5 high-resolution coupled climate model. *J. Climate*, *25*(8), 2755-2781. doi: 10.1175/JCLI-D-11-00316.1

Ferrari, R., & Ferreira, D. (2011). What processes drive the ocean heat transport? *Ocean Model.*, *38*(3–4), 171 - 186. doi: 10.1016/j.ocemod.2011.02.013

Ferrari, R., Nadeau, L.-P., Marshall, D. P., Allison, L. C., & Johnson, H. L. (2017). A model of the ocean overturning circulation with two closed basins and a re-entrant channel. *J. Phys. Oceanogr.*, *47*, 2887-2906. doi: 10.1175/JPO-D-16-0223.1

Ferrari, R., & Wunsch, C. (2009). Ocean circulation kinetic energy: Reservoirs, sources, and sinks. *Annu. Rev. Fluid Mech.*, *41*, 253-282. doi: 10.1146/annurev.fluid.40.111406.102139

Forget, G., & Ferreira, D. (2019, April). Global ocean heat transport dominated by heat export from the tropical Pacific. *Nature Geoscience*. doi: 10.1038/s41561-019-0333-7

Fox-Kemper, B., Ferrari, R., & Hallberg, R. (2008). Parameterization of mixed layer eddies. Part I: Theory and diagnosis. *J. Phys. Oceanogr.*, *38*(6), 1145–1165. doi: 10.1175/2007JPO3792.1

Ganachaud, A., & Wunsch, C. (2003). Large-scale ocean heat and freshwater transports during the World Ocean Circulation Experiment. *J. Climate*, *16*(4), 696-705. doi: 10.1175/1520-0442(2003)016⟨0696:LSOHAF⟩2.0.CO;2

Gnanadesikan, A. (1999). A simple predictive model for the structure of the oceanic pycnocline. *Science*, *283*(5410), 2077–2079. doi: 10.1126/science.283.5410.2077

Gordon, A. L. (1986). Interocean exchange of thermocline water. *J. Geophys. Res.*, *91*(C4), 5037-5046. doi: 10.1029/JC091iC04p05037

Gordon, A. L., Weiss, R. F., Smethie Jr., W. M., & Warner, M. J. (1992). Thermocline and intermediate water communication between the south Atlantic and Indian oceans. *J. Geophys. Res.*, *97*(C5), 7223-7240. doi: 10.1029/92JC00485

Greatbatch, R. J., & Zhai, X. (2007). The generalized heat function. *Geophys. Res. Lett.*, *34*(21). (L21601) doi: 10.1029/2007GL031427

Gregory, J. M. (2000, Jul 01). Vertical heat transports in the ocean and their effect on time-dependent climate change. *Climate Dynamics*, *16*(7), 501–515. doi: 10.1007/s003820000059

Griffies, S. M. (1998). The Gent-McWilliams skew flux. *J. Phys. Oceanogr.*, *28*(5), 831-841. doi: 10.1175/1520-0485(1998)028⟨0831:TGMSF⟩2.0.CO;2

Hieronymus, M., Nilsson, J., & Nycander, J. (2014). Water mass transformation in salinity-temperature space. *J. Phys. Oceanogr.*, *44*(9), 2547-2568. doi: 10.1175/JPO-D-13-0257.1

Hieronymus, M., Nycander, J., Nilsson, J., Döös, K., & Hallberg, R. (2019). Oceanic overturning and heat transport: The role of background diffusivity. *J. Climate*, *32*(3), 701-716. doi: 10.1175/JCLI-D-18-0438.1

Hochet, A., & Tailleux, R. (2019). Comments on "Diathermal heat transport in a global ocean model". *J. Phys. Oceanogr.*, *49*(8), 2189-2193. doi: 10.1175/JPO-D-19-0055.1

Holmes, R. M., Zika, J. D., & England, M. H. (2019a). Diathermal heat transport in a global ocean model. *J. Phys. Oceanogr.*, *49*(1), 141-161. doi: 10.1175/JPO-D-18-0098.1

Holmes, R. M., Zika, J. D., & England, M. H. (2019b). Reply to 'Comments on "Diathermal heat transport in a global ocean model"'. *J. Phys. Oceanogr.*, *49*(8), 2195-2197. doi: 10.1175/JPO-D-19-0139.1

Klinger, B. A., & Marotzke, J. (2000). Meridional heat transport by the subtropical cell. *J. Phys. Oceanogr.*, *30*(4), 696-705. doi: 10.1175/1520-0485(2000)030⟨0696:MHTBTS⟩2.0.CO;2

Large, W., & Yeager, S. (2004). *Diurnal to decadal global forcing for ocean and sea-ice models: the data sets and flux climatologies.* National Center for Atmospheric Research.

Large, W. G., McWilliams, J. C., & Doney, S. C. (1994). Oceanic vertical mixing: A review and a model with a nonlocal boundary layer parameterization. *Rev. Geophys.*, *32*(4), 363–403. doi: 10.1029/94RG01872

Large, W. G., & Yeager, S. G. (2009). The global climatology of an interannually varying air–sea flux data set. *Climate Dynamics*, *33*(2), 341–364. doi: 10.1007/s00382-008-0441-3

Lee, S.-K., Lumpkin, R., Baringer, M. O., Meinen, C. S., Goes, M., Dong, S., ... Yeager, S. G. (2018). Global meridional overturning circulation inferred from a data-constrained ocean & sea-ice model. *Geophys. Res. Lett.*. doi: 10.1029/2018GL080940

Marshall, J., & Speer, K. (2012). Closure of the meridional overturning circulation through Southern Ocean upwelling. *Nature Geosci*, *5*(3), 171-180. doi: 10.1038/ngeo1391

McDougall, T. J. (2003). Potential enthalpy: A conservative oceanic variable for evaluating heat content and heat fluxes. *J. Phys. Oceanogr.*, *33*(5), 945-963. doi: 10.1175/1520-0485(2003)033⟨0945:PEACOV⟩2.0.CO;2

Newsom, E. R., & Thompson, A. F. (2018). Reassessing the role of the Indo-Pacific in the ocean's global overturning circulation. *Geophys. Res. Lett.*, *45*(22), 12,422-12,431. doi: 10.1029/2018GL080350

Niiler, P., & Stevenson, J. (1982). The heat budget of tropical ocean warm-water pools. *J. Mar. Res*, *40*, 465–480.

Rintoul, S. R. (1991). South atlantic interbasin exchange. *J. Geophys. Res.*, *96*(C2), 2675-2692. doi: 10.1029/90JC02422

Saenko, O. A., Yang, D., & Gregory, J. M. (2018). Impact of mesoscale eddy transfer on heat uptake in an eddy-parameterizing ocean model. *J. Climate*, *31*(20), 8589-8606. doi: 10.1175/JCLI-D-18-0186.1

Simmons, H. L., Jayne, S. R., Laurent, L. C. S., & Weaver, A. J. (2004). Tidally driven mixing in a numerical model of the ocean general circulation. *Ocean Model.*, *6*(3), 245–263. doi: 10.1016/S1463-5003(03)00011-8

Speer, K., & Tziperman, E. (1992). Rates of water mass formation in the north Atlantic ocean. *J. Phys. Oceanogr.*, *22*(1), 93–104. doi: 10.1175/1520-0485(1992)022⟨0093:ROWMFI⟩2.0.CO;2

Speich, S., Blanke, B., & Cai, W. (2007). Atlantic meridional overturning circulation and the Southern Hemisphere supergyre. *Geophys. Res. Lett.*, *34*(23). doi: 10.1029/2007GL031583

Suresh, A., & Huynh, H. (1997). Accurate monotonicity-preserving schemes with Runge-Kutta time stepping. *J. Comput. Phys.*, *136*(1), 83 - 99. doi: 10.1006/jcph.1997.5745

Talley, L. (2013). Closure of the global overturning circulation through the Indian, Pacific, and Southern Oceans: Schematics and transports. *Oceanography*, *26*.

Talley, L. D. (2003). Shallow, intermediate, and deep overturning components of the global heat budget. *J. Phys. Oceanogr.*, *33*(3), 530-560. doi: 10.1175/1520-0485(2003)033⟨0530:SIADOC⟩2.0.CO;2

Thompson, A. F., Stewart, A. L., & Bischoff, T. (2016). A multi-basin residual-mean model for the global overturning circulation. *J. Phys. Oceanogr.*, *0*(0), null. doi: 10.1175/JPO-D-15-0204.1

Toggweiler, J. R., Druffel, E. R. M., Key, R. M., & Galbraith, E. D. (2019). Upwelling in the ocean basins north of the ACC Part 2: How cool subantarctic water reaches the surface in the tropics. *J. Geophys. Res.*, *0*(ja). doi: 10.1029/2018JC014795

Trenberth, K. E., & Caron, J. M. (2001). Estimates of meridional atmosphere and ocean heat transports. *J. Climate*, *14*(16), 3433–3443. doi: 10.1175/1520-0442(2001)014⟨3433:EOMAAO⟩2.0.CO;2

Trenberth, K. E., Zhang, Y., Fasullo, J. T., & Cheng, L. (2019). Observation-based estimates of global and basin ocean meridional heat transport time series. *J. Climate*, *32*(14), 4567-4583. doi: 10.1175/JCLI-D-18-0872.1

Valdivieso, M., Haines, K., Balmaseda, M., Chang, Y.-S., Drevillon, M., Ferry, N., … Andrew Peterson, K. (2017). An assessment of air–sea heat fluxes from ocean and coupled reanalyses. *Climate Dynamics*, *49*(3), 983–1008. doi: 10.1007/s00382-015-2843-3

Vallis, G. K., & Farneti, R. (2009). Meridional energy transport in the coupled atmosphere–ocean system: Scaling and numerical experiments. *Q. J. Roy. Meteorol. Soc.*, *135*(644), 1643–1660.

Vranes, K., Gordon, A. L., & Ffield, A. (2002). The heat transport of the Indonesian Throughflow and implications for the Indian Ocean heat budget. *Deep Sea Research Part II: Topical Studies in Oceanography*, *49*(7), 1391 - 1410. doi: 10.1016/S0967-0645(01)00150-3

Woodgate, R. A. (2018). Increases in the Pacific inflow to the Arctic from 1990 to 2015, and insights into seasonal trends and driving mechanisms from year-round Bering Strait mooring data. *Progress in Oceanography*, *160*, 124–154. doi: 10.1016/j.pocean.2017.12.007

Yang, H., Li, Q., Wang, K., Sun, Y., & Sun, D. (2015). Decomposing the meridional heat transport in the climate system. *Climate Dynamics*, *44*(9), 2751–2768. doi: 10.1007/s00382-014-2380-5

Zika, J. D., Laliberté, F., Mudryk, L. R., Sijp, W. P., & Nurser, A. J. G. (2015). Changes in ocean vertical heat transport with global warming. *Geophys. Res. Lett.*, *42*(12), 4940–4948. doi: 10.1002/2015GL064156

Zika, J. D., Sijp, W. P., & England, M. H. (2013). Vertical heat transport by ocean circulation and the role of mechanical and haline forcing. *J. Phys. Oceanogr.*, *43*(10), 2095-2112. doi: 10.1175/JPO-D-12-0179.1